Nonlinear Ultrasonic Phased Array Imaging

J. N. Potter,* A. J. Croxford, and P. D. Wilcox
Faculty of Engineering, University of Bristol, Queen's Building, University Walk, Bristol BS8 1TR, United Kingdom
(Received 14 February 2014; published 3 October 2014)

This Letter reports a technique for the imaging of acoustic nonlinearity. By contrasting the energy of the diffuse field produced through the focusing of an ultrasonic array by delayed parallel element transmission with that produced by postprocessing of sequential transmission data, acoustic nonlinearity local to the focal point is measured. Spatially isolated wave distortion is inferred without requiring interrogation of the wave at the inspection point, thereby allowing nonlinear imaging through depth.

DOI: 10.1103/PhysRevLett.113.144301 PACS numbers: 43.25.+y, 62.20.mt, 62.30.+d

Introduction.—Despite the sensitivity of acoustic nonlinearity to material microstructure [1–3], mechanical damage [4,5] and tissue pathology [6,7] having long been known, the lack of effective nonlinear acoustic imaging has held back the practical use of this important modality. The lack of progress in this field is primarily due to the difficulty in spatially isolating the source of wave distortion due to acoustic nonlinearity since the wave is not accessible by measurement systems at all points. Most measurements of acoustic nonlinearity have, therefore, been limited to spatially averaged values [8] or implicit localization through exhaustive tomographical methods [9–11]. Few explicit techniques have been proposed for the imaging of acoustic nonlinearity. Those that have require optical interrogation of the inspection point [12,13] and are consequently limited to surface measurements, which precludes their use in many applications.

Conversely, linear acoustic imaging has long been made tractable by the use of ultrasonic phased arrays. Through the application of relative delays to the parallel transmission of discrete elements, beam forming may be controlled, typically to achieve steering or focusing. More recently, an alternative approach to array imaging commonly referred to as full matrix capture has been employed [14]. Here, rather than transmitting on elements in parallel, time-domain responses from all transmitter-receiver pair combinations are acquired sequentially to yield the so-called full matrix of data. Delay laws are then applied in postprocessing to emulate the equivalent delayed parallel transmission. The work reported here identifies how differences in the wave propagation of these transmissions techniques can be used to image acoustic nonlinearity.

Herein, the focusing of ultrasound through postprocessing of sequential transmissions and physical focusing through parallel element transmission shall be referred to as *sequential* and *parallel* focusing, respectively. Although these two approaches are linearly equivalent, the same is not true of nonlinear propagation. When performing parallel focusing, the absolute acoustic pressure seen by the material is higher at the focal point than in any of the individual transmission cycles during the equivalent sequential focusing. Consequently, there is a larger transfer of energy from the fundamental harmonic to other frequencies due to nonlinear phenomena at the focal point in the parallel focusing case.

The proposed technique infers acoustic nonlinearity at the focal point by measuring the relative energy of the transmission frequency band within the diffuse field for parallel and sequential focusing. This parameter is related to acoustic nonlinearity at the focal point as a consequence of two phenomena. First, energy sampled at any point within the diffuse field is proportional to the total energy in the system. Second, since transmission, linear propagation, and nonlinear self-interaction are the same for the two focusing methods, relative differences in energy within the transmission bandwidth are restricted to nonlinear losses occurring local to the focal point. A measurement of relative energy of the transmission bandwidth within the diffuse field, therefore, provides a measure of acoustic nonlinearity at the focal point.

The implementation requires only a single ultrasonic array and knowledge of acoustic velocity within a material. Since these requisites are the same as for linear imaging, the proposed nonlinear imaging modality is immediately available to many applications where linear ultrasonic array imaging is currently applied.

Nonlinear array imaging method.—Consider, for example, the case of longitudinal wave propagation through an elastic solid with an isotropic bulk nonlinearity truncated to the second order. For the parallel and sequentially focused transmission of an N element array, the absolute wave amplitude U experienced at the focal point differs by a factor of N. The amplitude of second-harmonic waves generated is proportional to U^2, and hence, the amount of energy lost from the fundamental wave is proportional to U^4. The acoustic energy lost from the fundamental wave for the single transmission cycle in parallel focusing is, therefore, N^3 greater than that lost through the summation of the N transmission cycles necessary for the equivalent

sequential focusing. Given that ultrasonic arrays with order $N = 100$ elements are now commonplace, the difference in nonlinear energy loss from the fundamental between parallel and sequential focusing is significant and measurable. Furthermore, because the physical amplitude difference between parallel and sequential focusing is only large close to the focal point the difference in energy loss from the transmission frequency band is predominantly local to this point. This is the reason why the proposed technique is able to spatially map nonlinearity. It is important to note that this could not be achieved by simply applying parallel focusing at two different amplitudes. In that case, amplitude scaling between the two transmissions is experienced along the whole wave propagation path, rather than just at the focal point, resulting in much poorer nonlinear localization. Furthermore, the obtained measurements would not separate instrument and material nonlinearity.

More generally, even restricting consideration to low-order nonlinear dynamics, sonification of common nonlinear media will generate not only harmonics but also subharmonics and frequencies corresponding to sum and difference combinations of the transmission bandwidth [15–17]. The property common to all these nonlinear processes is a transfer of energy from the incident frequency band. Consequently, inspection of the fundamental frequency provides a metric sensitive to a wide range of acoustic nonlinearity.

The task here is to measure the relative loss in energy from the transmission frequency band at the focal point and focal time for parallel and sequential focusing. As the wave field in the system at the focal point is inaccessible to the measurement system, the loss in energy at the focal point must be inferred from the subsequent behavior of the system.

Linear propagation is the same for the two transmission types, meaning effects of interference on apparent acoustic energy are the same. Transmission energy is also the same for both fields, including effects of instrumentation nonlinearity and nonlinear contact-acoustic effects at the array-specimen interface. Furthermore, away from the focal point where there is no interference between element transmissions, losses of energy from the transmission frequency due to nonlinear self-interaction are the same. Differences in energy within the transmission band are only introduced due to relative amplitude scaling local to the focal point and time. The relative nonlinear energy loss at focal point may thereby be obtained by evaluating the difference in the *total* acoustic energy in the system for the two focusing methods at any instant after the focal time. To this end, the subsequent diffuse field is examined.

Within a theoretically ideal diffuse field, the expected root-mean-squared acoustic pressure will be the same at all points and the flux of acoustic energy in any direction is equally probable. In practice, diffuse fieldlike conditions are reached some time after an initial coherent excitation due to multiple scattering from grain and specimen boundaries. The acoustic energy at any point in the diffuse field is proportional to the total energy in the system at that time. Consequently, despite the relative nonlinear energy loss from the focal point being present only within subset of the propagating coherent field, it exists uniformly in the diffuse field. The difference in energy at any point in the diffuse field for parallel and sequential focusing, therefore, provides an approximation to the energy difference at the focal point and focal time, which in turn provides a measure of acoustic nonlinearity at that point.

The acoustic field will converge on the diffuse state as time increases. However, since propagation is dissipative, the signal to noise ratio will decrease with time. Furthermore, since received sequentially focused data are of lower amplitude, they will be degraded by incoherent noise to a greater extent than the parallel data, reducing the efficacy of diffuse energy comparisons as the delay between transmission and data acquisition increases. Consequently, the choice of this reception delay t_r is a compromise between maximizing amplitude and diffuse field convergence. Since the diffuse field is only static in a statistical sense, the energy value used should be the integral of that within a captured window, such that energy is evaluated between times t_r and $t_r + T$, where T is the window length.

The final consideration is that of frequency bandwidth. Increasing bandwidth will increase the acoustic energy incident at the focal point in addition to broadening sensitivity to a wider range of acoustic nonlinearity. However, any internal movement of energy within the band will not contribute to the measured value of nonlinearity. The evaluated bandwidth should, therefore, be the maximum for which there is no internal movement of energy. Noting the possible energy transfer to harmonics, subharmonics, sum, and difference frequencies, this corresponds to a value of two-thirds of the center frequency ω_0.

Let $f_{j,k}(t)$ be the time-domain signal received on element k for the sequential transmission of element j. $\delta_j(\bar{r})$ is the delay applied to the jth element to focus at point $\bar{r}$ (illustrated graphically in Fig. 1). $h_k(\bar{r}, t)$ is the time-domain received data on element k for the parallel transmission of all elements delayed by $\delta_j(\bar{r})$. The frequency ω spectra of $f_{j,k}(t)$ and $h_k(\bar{r}, t)$ within the time window t_r to $t_r + T$ are evaluated as $F_{j,k}(\omega) = \int_{t_r}^{t_r+T} f_{j,k}(t)e^{-i\omega t}dt$ and $H_k(\omega) = \int_{t_r}^{t_r+T} h_k(t)e^{-i\omega t}dt$, respectively.

For an N element array, assuming a received value proportional to displacement, the diffuse acoustic kinetic energy in the sequential focusing case E_S for focal position $\bar{r}$ is calculated as follows,

$$E_S(\bar{r}) = \sum_{k=1}^{N} \left(\int_{\frac{2}{3}\omega_0}^{\frac{4}{3}\omega_0} \omega^2 \left| \sum_{j=1}^{N} F_{j,k}(\omega) e^{i\omega\delta_j(\bar{r})} \right|^2 d\omega \right). \quad (1)$$

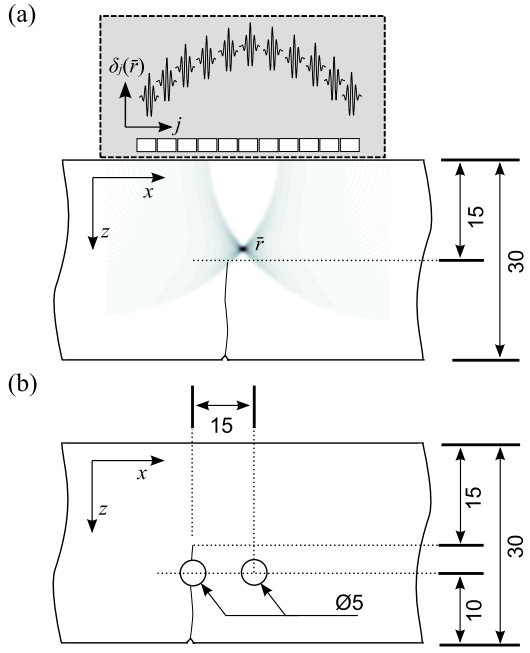

FIG. 1 (color online). Schematic of nonlinear array inspection configuration for (a) isolated fatigue crack and (b) fatigue crack and linear scatterers (dimensions in mm).

Similarly, the parallel transmission energy E_P is given by

$$E_P(\bar{r}) = \sum_{k=1}^{N} \left(\int_{\frac{2}{3}\omega_0}^{\frac{4}{3}\omega_0} \omega^2 |H_k(\bar{r},\omega)|^2 d\omega \right). \quad (2)$$

The nonlinear metric γ is defined to be the normalized difference between the sequential and parallel transmission energies as follows,

$$\gamma(\bar{r}) = \frac{E_S(\bar{r}) - E_P(\bar{r})}{E_S(\bar{r})}, \quad (3)$$

which represents the proportional energy loss from the transmission frequency band due to the nonlinear effects. Equivalent time-domain definitions of these parameters are given in the Supplemental Material [18].

Experimental fatigue crack imaging.—In order to evaluate the efficacy of the proposed technique, it is applied to fatigue cracks grown in Al2014 compact test specimens, which provide acoustic nonlinearity in a known location and the imaging of which represents an unsolved research problem of critical importance. Fatigue cracks exhibit complicated nonlinear mechanics that have been examined extensively elsewhere [4]. The nonlinear response can be expected to include even harmonic generation from local plasticity, subharmonic generation and frequency intermodulation from contact-acoustic "clapping" nonlinearity, and nonlinear frictional losses, all of which will result in a relative reduction in parallel diffuse energy within the transmission bandwidth and, consequently, an increase in the imaging metric.

For the first inspection configuration, as shown in Fig. 1(a), a 64 element, 5 MHz array was gel coupled to the surface parallel to that of crack initiation and positioned centrally over the crack. Assuming uniform acoustic velocity, the transmission delays are evaluated as $\delta_j(\bar{r}) = |\bar{r} - \bar{a}_j|/c_l$, where $\bar{a}_j$ is the location of transmitting element j. The material longitudinal velocity c_l was measured to be 6270 m/s. See the Supplemental Material [18] for a full description of specimen preparation, instrumentation, and experimental procedure.

Images of the absolute energy for $t_r = 1$ ms and $T = 120$ μs obtained through sequential transmission E_S and parallel transmission E_P are shown in Figs. 2(a) and 2(b), respectively. To the eye, these images appear identical, and the crack cannot be discerned through evaluation of either image individually. The dominant features of these images are produced as a consequence of linear scattering and as such are dependent on specimen geometry and reception delay; these features arise because the fields have not reached a genuinely diffuse state.

The normalized difference between the absolute energy images is taken to produce the nonlinear image shown in Fig. 2(c). The crack becomes clearly visible in the nonlinear image. The amplitude of γ increases local to the crack, signifying a proportionately higher loss of energy from the parallel transmission in comparison to the sequential transmission case. The amplitude is largest towards the tip of the crack, which is consistent with imaging of contact acoustic nonlinearity where the interface is most completely closed. Note that the observed features of the absolute energy images do not appear in the nonlinear image. Despite the absolute energy images changing with reception time, only the signal to noise ratio of the nonlinear image is dependent on reception time and not the characteristic shape.

A comparative linear image is shown in Fig. 2(d), plotted on a dB scale, where 0 dB is defined as the peak amplitude in the image, to better resolve the crack. This was produced using the total focusing method (TFM) [14], which applies focusing in both transmission and reception to each pixel in the image and represents close to the theoretical maximum linear imaging performance.

The crack is visible as a consequence of weak scattering from contact points along the crack interface. Although the presence of the crack is detectable linearly, accurate imaging of its geometry is not possible. Significantly, the nonlinear image more closely matches the location of the crack tip as measured at the surface (shown by a cross in Fig. 2).

Another significant feature that should be noted is the absence of signal from the back wall of the sample in the nonlinear image, which appears as the most dominant feature in the linear image. This highlights one of the most important properties of the proposed technique, the full

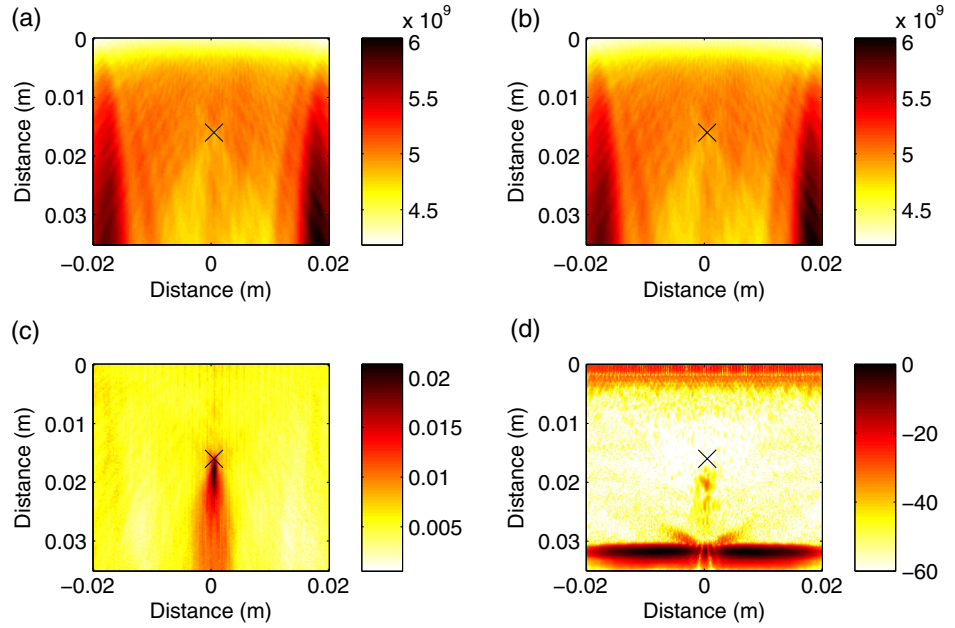

FIG. 2 (color online). Fatigue crack images. (a) Sequential transmission energy E_S (arb. units), (b) parallel transmission energy E_P (arb. units), (c) nonlinear metric (γ), and (d) linear TFM image (dB).

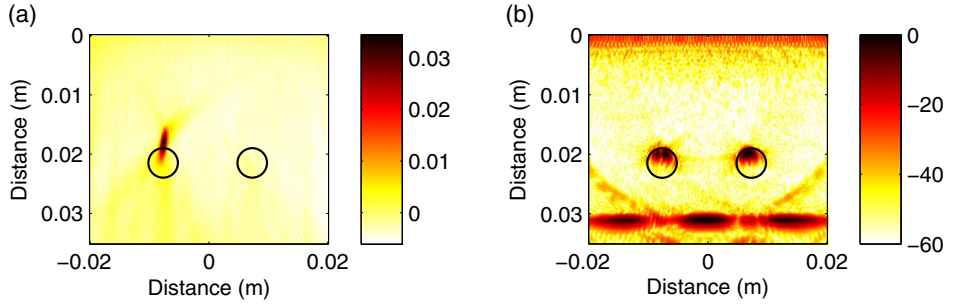

FIG. 3 (color online). Fatigue crack with linear scatterer images. (a) Nonlinear metric (γ) and (b) linear TFM (dB).

separation of nonlinear and linear acoustic modalities. Commonly, an acoustic feature of interest will be in close proximity to a strong linear scatterer such as the case of crack growth initiated by stress concentration at some geometric feature. Whereas a linear image will be dominated by scattering from the local geometry, potentially masking the presence of a crack, nonlinear imaging will only show the feature of interest.

To demonstrate this, another test was conducted in which a 5 mm diameter hole was machined behind the crack tip of a similar fatigue specimen, such that the crack extends approximately 2.5 mm beyond the boundary of the hole, as shown in Fig. 1(b). This emulates early stage fatigue crack growth from a geometric feature such as a fixing hole. As a reference, an identical hole was positioned 15 mm away at the same depth in the specimen.

The generated nonlinear image is shown in Fig. 3(a), in which the hole locations are highlighted with circles. Since the technique is not dependent on scattering, neither of the holes are imaged and only the nonlinear crack is visible. This is compared to a linear TFM image in Fig. 3(b). Here, the fatigue crack cannot be resolved, with linear scattering from both holes dominating the image.

The results presented here clearly demonstrate the capability of the proposed technique to locally image acoustic nonlinearity. This method advances the measurement of acoustic nonlinearity to an easily acquirable and effective imaging modality with the potential to both enhance existing imaging and provide sensitivity to previously undetectable physical features.

This work was supported by the UK Research Centre in Non-destructive Evaluation (RCNDE).

*jack.potter@bristol.ac.uk

[1] A. J. Croxford, P. D. Wilcox, B. W. Drinkwater, and P. B. Nagy, J. Acoust. Soc. Am. **126**, EL117 (2009).
[2] P. B. Nagy, Ultrasonics **36**, 375 (1998).

[3] J. H. Cantrell and W. T. Yost, International Journal of Fatigue **23**, 487 (2001).
[4] I. Y. Solodov and B. A. Korshak, Phys. Rev. Lett. **88**, 014303 (2001).
[5] Y. Ohara, T. Mihara, R. Sasaki, T. Ogata, S. Yamamoto, Y. Kishimoto, and K. Yamanaka, Appl. Phys. Lett. **90**, 011902 (2007).
[6] F. A. Duck, *Physical Properties of Tissue: a Comprehensive Reference Book* (Academic Press, New York, 1990).
[7] J. Zhang and F. Dunn, J. Acoust. Soc. Am. **81**, 1635 (1987).
[8] M. A. Averkiou, D. N. Roundhill, and J. E. Powers, IEEE Ultrasonics Symposium **2**, 1561 (1997).
[9] A. Cai, J. Sun, and G. Wade, IEEE Trans. Ultrason. Ferroelectr. Freq. Control **39**, 708 (1992).
[10] X. Gong, D. Zhang, J. Liu, H. Wang, Y. Yan, and X. Xu, J. Acoust. Soc. Am. **116**, 1819 (2004).
[11] Y. Nakagawa, M. Nakagawa, M. Yoneyama, and M. Kikuchi, in *Acoustical Imaging*, edited by A. Berkhout, J. Ridder, and L. Wal (Springer, New York, 1985), Vol. 14, pp. 595–604.
[12] T. J. Ulrich, P. A. Johnson, and R. A. Guyer, Phys. Rev. Lett. **98**, 104301 (2007).
[13] I. Solodov, J. Wackerl, K. Pfleiderer, and G. Busse, Appl. Phys. Lett. **84**, 5386 (2004).
[14] C. Holmes, B. W. Drinkwater, and P. D. Wilcox, NDT & E Int. **38**, 701 (2005).
[15] V. V. Kazakov, Appl. Phys. Lett. **81**, 646 (2002).
[16] A. Moussatov, V. Gusev, and B. Castagnede, Phys. Rev. Lett. **90**, 124301 (2003).
[17] I. Y. Solodov, N. Kron, and G. Busse, Ultrasonics **40**, 621 (2002).
[18] See the Supplemental Material at http://link.aps.org/supplemental/10.1103/PhysRevLett.113.144301 for a time-domain representation of the presented parameters and a full description of specimen preparation, instrumentation, and experimental procedure.